# Encyclopaedia of Rock Mechanics in Civil and Environmental Engineering

Contributors | **Lixin Wu, Meng Wang, and Mahdi Rasouli Maleki et al.**

# Encyclopaedia of
# ROCK MECHANICS IN CIVIL AND ENVIRONMENTAL ENGINEERIN

## Volume I: Fundamentals of Rock Mechanics


Contributors

**Lixin Wu, Meng Wang and Mahdi Rasouli Maleki et al.**



AURIS
Reference

www.aurisreference.com

# Encyclopaedia of Rock Mechanics in Civil and Environmental Engineering

## Volume I: Fundamentals of Rock Mechanics

Contributors: Lixin Wu, Meng Wang and Mahdi Rasouli Maleki et al.

**Published by Auris Reference Limited**

**www.aurisreference.com**

United Kingdom



**Fundamentals of Rock Mechanics**

ISBN: 978-1-78154-903-2 (Set of 3 Volumes)

British Library Cataloguing in Publication Data
A CIP record for this book is available from the British Library

Printed in the United Kingdom

# Encyclopaedia of ROCK MECHANICS IN CIVIL AND ENVIRONMENTAL ENGINEERING

# List of Abbreviations

| | |
|---|---|
| AE | Acoustic Emission |
| AMS | Anisotropy of Magnetic Susceptibility |
| ASTM | American Society for Testing and Materials |
| BPS | Buried Pressure Sensor |
| CFP | Close Field Photogrammetry |
| COA | Crack Optical Acquirement |
| DCS | Degree of Capillary Saturation |
| DRM | Detrital Remanent Magnetization |
| EDZ | Excavation Disturbed Zone |
| ESTCS | Exploiting Extremely Steep and Thick Coal Seams |
| HDD | Horizontal Directional Drillholes |
| HPHT | High Pressure/High Temperature |
| IRR | Infrared Radiation |
| ISRM | International Society for Rock Mechanics |
| LTCC | Longwall Top Coal Caving |
| NRM | Natural Remanent Magnetization |
| PAFD | Progressive Alternating Field Demagnetization |
| RQD | Rock Quality Designation |
| RSO | Roof Separation Observation |
| RSRM | Remote Sensing Rock Mechanics |
| SCL | Sprayed Concrete Tunnel Linings |
| SEM | Scanning Electron Microscope |
| SHS | Simulated Hydraulic Support |
| SPATE | Stress Pattern Analysis by Thermal Emission |
| SSTCC | Sub Horizontal Section Top Coal Caving |
| TIR | Thermal Infrared |
| TSA | Thermo Elastic Stress Analysis |

# List of Contributors

**Lixin Wu**
Academy of Disaster Reduction & Emergency Management, Beijing Normal University, Beijing, China
Institute for Geo-informatics & Digital Mine Research, Northeastern University, Shenyang, China

**Shanjun Liu**
Institute for Geo-informatics & Digital Mine Research, Northeastern University, Shenyang, China

**Karl Gunnar Holter**
Department of Geology and Mineral Resources Engineering, Norwegian University of Science and Technology, Sem Sælands vei 1, 7491 Trondheim, Norway

**Md. Aminul Islam**
Department of Petroleum Engineering and Applied Geophysics, Norwegian University of Science and Technology, Trondheim, Norway

**Paal Skalle**
Department of Petroleum Engineering and Applied Geophysics, Norwegian University of Science and Technology, Trondheim, Norway

**Yasuto Itoh**
Graduate School of Science, Osaka Prefecture University, Osaka, Japan

**Machiko Tamaki**
Japan Oil Engineering Co. Ltd., Tokyo, Japan

**Osamu Takano**
JAPEX Research Center, Japan Petroleum Exploration Co. Ltd., Chiba, Japan

**Irfan Celal Engin**
Afyon Kocatepe University, Engineering Faculty, Department of Mining Engineering, Afyonkarahisar, Turkey

**X. P. Lai**
School of Energy and Mining Engineering, Xi'an University of Science and Technology, Xi'an 710054, China

Key Laboratory of Western Mines and Hazard Prevention, Ministry of Education of China, Xi'an 710054, China

**P. F. Shan**
School of Energy and Mining Engineering, Xi'an University of Science and Technology, Xi'an 710054, China
Key Laboratory of Western Mines and Hazard Prevention, Ministry of Education of China, Xi'an 710054, China

**J. T. Cao**
School of Energy and Mining Engineering, Xi'an University of Science and Technology, Xi'an 710054, China
Key Laboratory of Western Mines and Hazard Prevention, Ministry of Education of China, Xi'an 710054, China

**F. Cui**
School of Energy and Mining Engineering, Xi'an University of Science and Technology, Xi'an 710054, China
Key Laboratory of Western Mines and Hazard Prevention, Ministry of Education of China, Xi'an 710054, China

**H. Sun**
School of Energy and Mining Engineering, Xi'an University of Science and Technology, Xi'an 710054, China
Key Laboratory of Western Mines and Hazard Prevention, Ministry of Education of China, Xi'an 710054, China

**Wing Kei Kong**
A-P Design, MWH Australia Pty Ltd, Level 3, 35 Boundary Street, South Brisbane, QLD 4101, Australia

# Preface

Encyclopaedia of Rock Mechanics in Civil and Environmental Engineering covers the necessary understanding and the key techniques supporting the rock engineering design of structural foundations, dams, rock slopes, wellbores, tunnels, caverns, hydroelectric schemes and mines. Rock mechanics today is closely associated with, and indeed part of, construction, energy, and environmental engineering. Rock mechanics is a theoretical and applied science of the mechanical behavior of rock and rock masses; compared to geology, it is that branch of mechanics concerned with the response of rock and rock masses to the force fields of their physical environment. The text *Fundamentals of Rock Mechanics* focuses on mechanical behavior of rock and rock masses, and presents the essentials of rock mechanics. First chapter focuses on remote sensing rock mechanics and earthquake thermal infrared anomalies. The performance of EVA-based membranes for SCL in hard rock has been measured in second chapter. The goal of third chapter is to provide additional insight regarding the organization of the non-linear model input parameters in borehole simulations and to assist other researchers involved in the rock physics-related research fields. In fourth chapter, we present preliminary results of rock magnetic analyses of the Cretaceous Yezo Supergroup, the Eocene Ishikari Group and the Miocene Kawabata formation in order to detect tectonic movements around the basin and to describe the microfabric of sedimentary rocks related to the tectonic regime and sedimentation processes in the mobile zone. Theories on rock cutting, grinding and polishing mechanisms have been proposed in fifth chapter. In sixth chapter, a methodology has been developed for assessing destabilization potential of the host rock mass from mine voids. Last chapter deals with water ingress assessment for rock tunnels.

# Contents

# Chapter 1

# REMOTE SENSING ROCK MECHANICS AND EARTHQUAKE THERMAL INFRARED ANOMALIES

Lixin Wu[1,2] and Shanjun Liu[2]

[1]Academy of Disaster Reduction & Emergency Management, Beijing Normal University, Beijing, China

[2]Institute for Geo-informatics & Digital Mine Research, Northeastern University, Shenyang, China

## INTRODUCTION

Rock fracturing is the cause of many geo-hazards including tectonic earthquake (EQ), rock burst, rock sloping and rock pillar failure. Radiation signals such as acoustic emission, radio frequency emission and electromagnetic (EM) radiation from loaded deforming rock, are able to provide useful information for monitoring, interpreting and predicting rock fracturing (Renata, 1977, Brady and Rowell, 1986,Yamada et al., 1989, Martelli et al., 1989). Based on thermo-elastic theory, thermo-elastic stress analysis (TSA) and stress pattern analysis by thermal emission (SPATE) were developed for the stress measurement of solid materials, including homogeneous metal, macromolecular and composite materials, respectively in 1960's and 1970's (Mounatin and Webber, 1978). Luong applied thermovision to study experimentally the damage processes of concrete and rock (Luong, 1990), but no reach to the remote sensing on geo-hazards.

In the experiments for investigating the mechanism of satellite thermal infrared (TIR) anomaly before tectonic EQ (Gorny et al., 1988, Qiang et al., 1990), it was discovered that there do exist TIR anomaly before rock fracturing (Geng et al., 1992). Later, it was furthermore discovered that there are obvious TIR features as precursors of rock fracturing, and that the loaded stress around

0.79 $\sigma_c$ can be taken as a precaution index for the stability monitoring of loaded rocks (Wu and Wang, 1998). To explore the laws of infrared radiation (IRR) variation in the process of rock loading, deforming and fracturing, and to reveal the possible mechanism of satellite TIR anomaly before EQ, a large amount of IRR imaging experiments on rock loaded to fracturing were conducted in China (Wu et al., 2000, 2001, 2002, 2003,2004a, 2004b, 2004c, 2004d, 2006a, 2006b; Deng et al., 2001, Liu et al., 2002). Hence, a new intersection discipline, Remote Sensing Rock Mechanics (RSRM), which takes Remote Sensing, Rock Mechanics, Rock Physics and Informatics as its foundations and serves for remote sensing on geo-hazards, was originated (Geng et al., 1992; Wu et al., 2000).

Based on retrospection to past experiments on RSRM, it was pointed out that there are two IRR anomalies, being IRR image anomaly and IRR temperature curve anomaly respectively, can act as rock fracturing precursors. The average IRR temperature (AIR*T*), being the integral reflection of surface IRR energy, is applied as a quantitative index to study the temporal evolution of IRR from loaded rock and to seek for the potential precursors of rock fracturing. The temporal evolution of AIR*T* are the comprehensive effect of a series of physical-mechanical processes inside a loaded rock, such as rock thermo-elastic acting, pore gas desorbing & escaping, fractures producing & extending, rock frictionating, heat transferring and environment radiation. The thermo-elastic effect and the frictional thermal are two of the main mechanisms of increased IRR from loaded rock. RSRM experiments had revealed the laws of changed IRR from loaded rock and provided scientific interpretations for the mechanisms of satellite TIR anomaly before tectonic EQs of Ms>5.5.

## REMOTE SENSING ROCK MECHANICS EXPERIMENTS

### Experiment Methods and Tools

The typical RSRM experiment is comprised of a loader (uni-axial or bi-axial), an infrared imager and rock samples. As in Figure 1, a bi-axial loader was applied for loading along two directions, and an infrared imager was applied to detect the surface IRR from loaded rock. The maximum imaging rate of the imager is 60f/s, and the recording rate was usually set as 1f/s to record the IRR images continuously. Usually, tectonic EQ might be resulted from the suddenly fracturing of compressively-sheared crust rock, the suddenly breaking of faults at disjointed zones, the suddenly sliding of compressively-sheared faults or the stability losing of compressively loaded intersected faults. To simulate the different mechanisms of rock fracturing and EQ, several typical loading schemes were applied as in Figure 1.

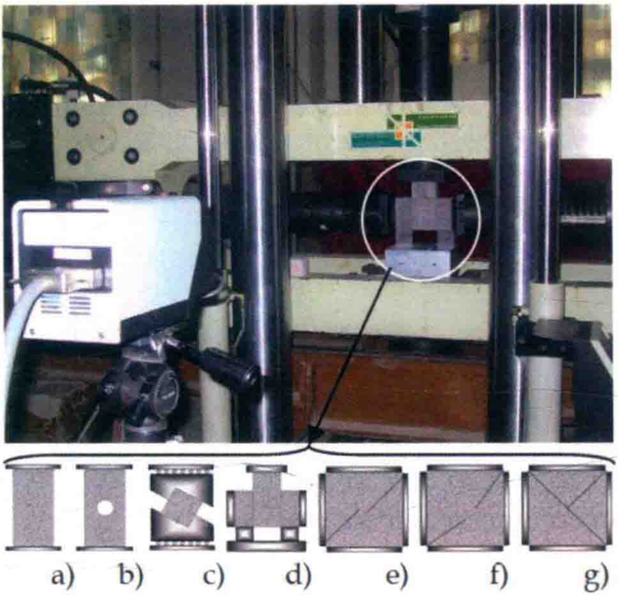


**Figure 1.** RSRM experiment schemes to simulate different mechanisms of rock fracturing or tectonic EQ: a) uni-axially load on a standard cylinder rock sample; b) uni-axially load on a cylinder rock sample with a central hole; c) compressively-sheared load on a hexahedral rock sample; d) bi-axially load on three jointed rock samples to frictional sliding; e) bi-axially load on a damage rock sample with en echelon faults; f) bi-axially load on a damage rock sample with disjointed faults; and g) bi-axially load on three jointed rock samples simulating intersected faults.

## Rock Fracturing Precursor: IRR Image Anomaly

### *Uni-axially Loaded Rock*

Lots of rock samples made from coal, ironstone, sandstone, marble, limestone, granite, granodiorite, gabbro and gneiss were uni-axially loaded and thermal imaging detected. The sample size was standard of diameter and length, respectively, 50 and 100mm. It was discovered that the IRR images of the uni-axially loaded rock have different features for different fracturing pattern (Wu et al., 2006a). As in Figures 2~4, there are three fracturing patterns, "X"-shaped, "//"-shaped and "|"-shaped respectively, occurred in our experiments. The "X"-shaped and "//"-shaped positive IRR abnormal strips foretell the coming of "X"-shaped shearing fracturing and the coming of "//"-shaped shearing fracturing respectively, while the "|"-shaped negative IRR abnormal strip foretells the coming of tensile fracturing.

The "X"-shaped positive IRR abnormal strips generated with loading along the "X"-shaped shearing zone before peak stress, and got distinguished after peak stress, as in Figure 2. The rock sample got finally fractured along the "X"-shape shearing zone. The evolution of IRR abnormal strip had also reflected the fracturing being not symmetrical upper-and lower, in that the upper part was clear with higher temperature, while the lower part is fuzzy with lower temperature.

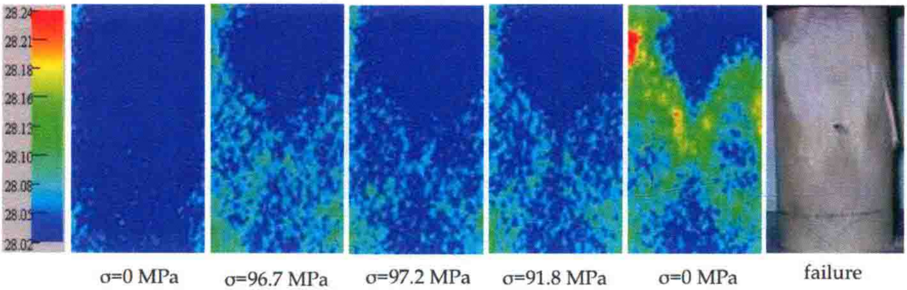


**Figure 2.** The IRR image positive anomaly of "X"-shaped shearing fracturing of an uni-axially loaded marble sample.

The "//"-shaped positive IRR abnormal strips generated with loading along the "//'-shaped shearing zone at the upper part of sample before peak stress, and got distinguished after peak stress, as in Fig 3. The evolution of the positive IRR image anomaly had also reflected the fracturing being not symmetrical in that the upper part of the IRR anomaly strip was clear with higher temperature, while the lower part was fuzzy excepting for the final fracturing near the bottom of the sample. Besides, there was strong IRR anomaly spot at the fracturing center for the intensive accumulation of mechanical energy and for the intensive generation of frictional thermal at the local central place.

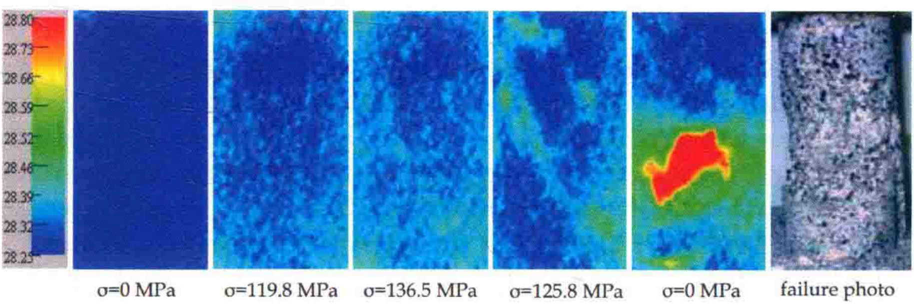


**Figure 3.** The IRR image positive anomaly of "//"-shaped shearing-fracturing of an uni-axially loaded granite sample.

The "|"-shaped negative IRR abnormal strip generated with loading along the tensile fracturing zone of a rock sample before the peak stress, and got distinguished gradually at the peak stress and after fracturing, as the approximately vertical dark strip in Figure 4. The same phenomenon for a sandstone sample with a calcite vein was also reported (Wu, et al., 2000).

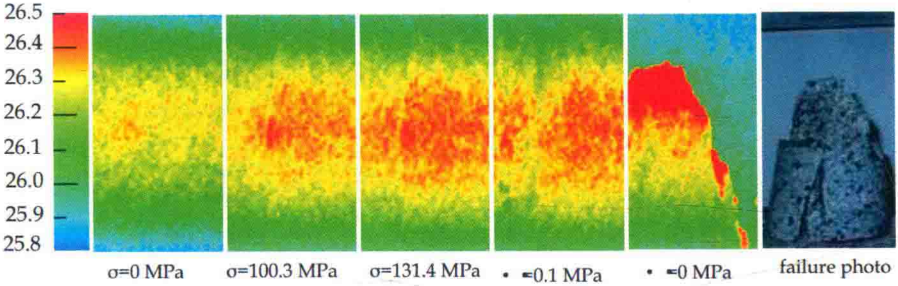


**Figure 4.** The IRR image negative anomaly of "|"-shaped tensile fracturing of an uni-axially loaded granite sample.

## *Uni-Axially Loaded Rock with a Central Hole*

More than 10 samples with a central hole, modeling the structure stability of loaded rock tunnels, made from marble and granite were infrared imaging detected. The rock samples had two kinds of shapes respectively being cylinder with diameter and length, respectively, 50 and 100mm, and regular block with thickness, width and length, respectively, 70, 35 and 100 mm. It was discovered that there were distinguished positive IRR image anomalies before rock fracturing, and the place of anomaly were exactly the coming fracturing place. As in Figure 5, the positive IRR image anomalies had reflected the two kinds of fracturing, respectively being diagonal fracturing (sample 1~5) and fork fracturing (sample 6). The IRR anomalies, along the fracturing planes and shaped as spots or strips, generated not only on rock surface but also on the hole's surface (lateral sample 4 and 5). The temperature increment is 1~3°C and 4~8°C respectively for marble and granite samples.

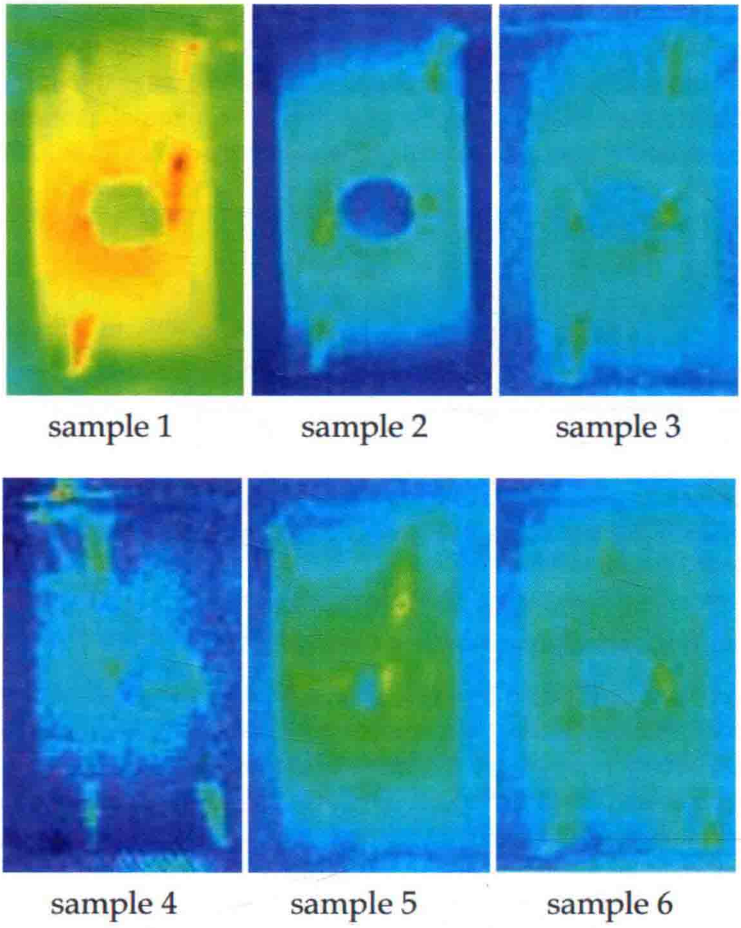


**Figure 5.** The IRR image positive anomalies of a group of uni-axially loaded marble samples with a central hole.

## *Compressively Sheared Rock*

More than 20 samples, size 7×7×7×cm$^3$, made from sandstone, marble, limestone, granite and gneiss, were compressively sheared and infrared imaging detected. Three pairs of steel platens with shearing angle being 45°, 60°and 70° respectively were applied. The loading rate was controlled as 2~5kN/s. It was discovered that the IRR temperature of rock surface changed with loading, and a strip-shaped positive IRR image anomaly generated along the central shearing plane before fracturing. With loading, the positive abnormal strip got more and more distinguished and migrated gradually from the upper end to the lower end of the sample, which foretold that the compressive-shearing fracturing was developing gradually from the upper end to the lower end of the sample along the central shear plane. Figure 6shows the typical IRR image series of a compressively sheared limestone sample.

As a special geological phenomenon occurring with the formation of great fault, penniform-shaped fractures are a group of secondary fractures produced with the formation of great primary fracture (Nicolas et al., 1977). It happened to occur in our experiments that there were penniform-shaped fractures produced with a primary fracture in the compressive loaded rock samples, as in Figure 7. The IRR positive anomaly strips generated aside the primary IRR strip, passing through the central shearing plane, had reflected the penniform-shaped fracturing events.

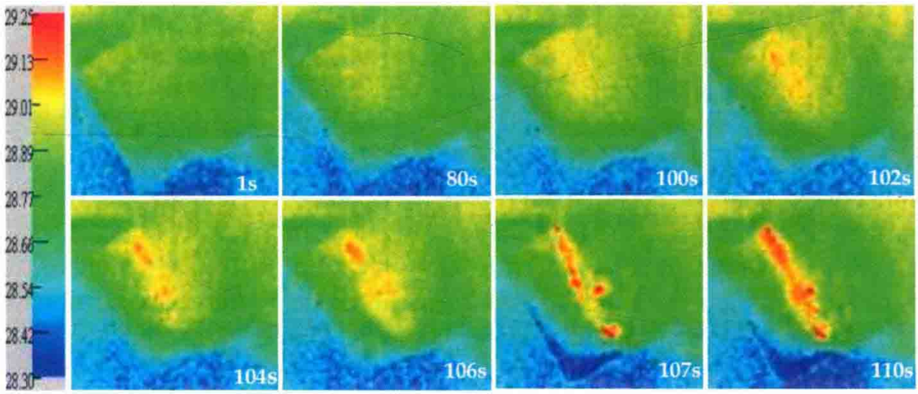


**Figure 6.** The IRR image positive anomaly of the fracturing of a compressively sheared limestone sample (time in second).

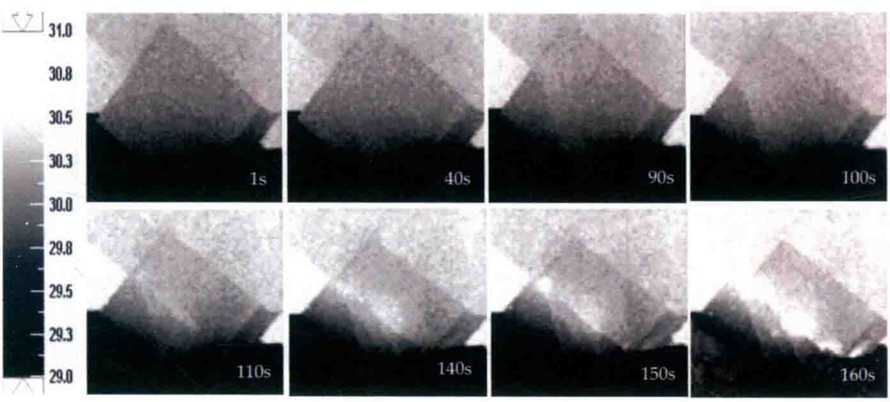


**Figure 7.** The IRR image anomaly of the penniform-shaped fracturing of a compressively sheared marble sample.

## *Bi-Sheared Frictional Sliding Rock Blocks*

Ten groups of rock samples made from gabbro, granodiorite, limestone and marble were IRR detected in the process of bi-sheared frictional sliding or viscosity sliding. Each group, as in Figure 8 and 9, was comprised of three jointed rock blocks whose size respectively be $50\times50\times100mm^3$, $50\times70\times150mm^3$and $50\times50\times100mm^3$ from left to right, and its friction area was constant, $50\times100mm^2$. Four contact conditions, symmetrical (yes for rock property and for its smooth friction surface, as in Figure 8), uncertain symmetrical (yes for rock property but not for its coarse friction surface, as in Figure 9), unstable asymmetrical (yes for rock property but not for its staged friction surface) and stable asymmetrical (not for rock property but yes for its smooth friction surface), were designed and tested respectively (Wu et al., 2004b).

It is revealed that the evolution of rock surface IRR temperature field is not only correlated with rock stress, but also correlated with the features of friction surface and rock properties at both sides. General law lies in that the IRR at the place of stress concentration and strong friction zone is stronger than that at the place of stress relaxation and weak friction zone. In condition of friction surface be symmetrical, the IRR image is double butterfly-wings shaped, as in Figure 8. However, in condition of friction surface be uncertain symmetrical, unstable asymmetrical or stable asymmetrical, the temporal-spatial evolution of IRR anomaly is uncertain or unstable, as in Figure 9. The positive IRR anomaly spots, foretelling the evolution of stress, energy and viscosity-sliding process, may be beads-shaped, needle-shaped, suspended needle-shaped, strip-shaped, single butterfly-wings shaped or its evolution in order (Wu et al., 2004b).

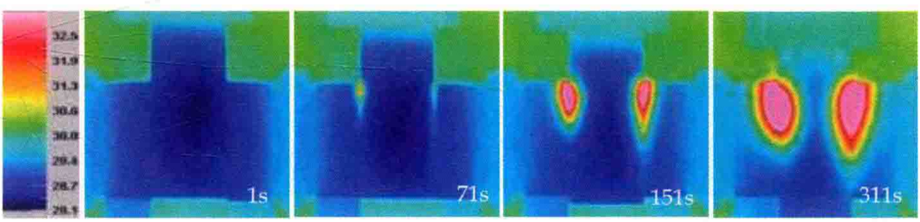


**Figure 8.** The IRR image positive anomaly of the stick-slipping of symmetrical rock samples (time in second).